ADVANCED MATERIALS INTERFACES

www.advmatinterfaces.de

Temperature Dependent Epitaxial Growth of C_{60} Overlayers on Single Crystal Pentacene

Yasuo Nakayama, Ryohei Tsuruta, Alexander Hinderhofer, Yuta Mizuno, Katharina Broch, Alexander Gerlach, Tomoyuki Koganezawa, Takuya Hosokai, and Frank Schreiber*

Heteroepitaxy of one material onto another molecular single crystal surface is one promising route for resolving questions about formation criteria of molecular heterojunction structures as well as for the development of next-generation organic electronic devices allowing efficient intermolecular charge carrier exchange. In the present work, the in-plane and out-of-plane crystallinity of an epitaxial molecular p–n heterojunction, C_{60} (acceptor) overlayers formed on the single crystal surface of pentacene (donor), and its evolution, depending on the growth temperature, are systematically elucidated. It is demonstrated that the crystallinity of the C_{60} on pentacene is dominated by the temperature during the growth rather than the postannealing of the sample. The mean crystallite size in the in-plane directions grows from 50 to 150 nm proportionally to the growth temperature in a range of 125–370 K. The present results suggest that the formation mechanisms of the C_{60}/pentacene heterojunction are kinetically controlled, by diffusion processes at the molecular interface, rather than by the thermal equilibrium conditions.

1. Introduction

Coherent arrangements of π-conjugated molecules are key requirements for pursuing efficient conduction of charge carriers inside organic electronic devices. On account of the formation of electronic bands and the associated delocalization of charge carriers,[1–3] reasonably high charge carrier mobility has been reported in devices of single crystalline organic semiconductors.[4–6] In the cases of donor–acceptor systems, the creation of well-ordered molecular assemblies is also regarded as a promising route for realizing efficient ambipolar organic field effect transistors through enhanced mobilities of both electrons and holes,[7–9] and for achieving improved power conversion efficiencies of organic photovoltaics through extended exciton diffusion lengths and promotion of electron–hole dissociation due to charge carrier delocalization.[10–14] Accordingly, accurate control of the crystal quality of molecular heterojunctions is desired for advancing further development of next-generation organic electronic devices.[15–17]

In the present work, the evolution of the crystallinity of a well-ordered bimolecular heterojunction, C_{60} on a single crystal surface of pentacene ($C_{22}H_{14}$), is studied depending on the growth temperature by means of surface X-ray diffraction techniques and noncontact mode atomic force microscopy (nc-AFM). Pentacene (**Figure 1**a) and C_{60} (Figure 1b) are representative p-type (donor) and n-type (acceptor) semiconducting compounds generating an exciton-dissociating interface in a prototypical organic solar cell device.[18] The pentacene/C_{60} interface has been studied widely, both experimentally[19–24] and theoretically.[25–30] It was recently discovered that C_{60} crystallizes in its bulk structure epitaxially by aligning the nearest-neighbor face-centered-cubic (fcc)-$<1\bar{1}0>$ axis uniquely along the $[1\bar{1}0]$ direction of the pentacene single crystal (Pn-SC) surface.[31] The type of this epitaxial interface is categorized into the incommensurism, whereas it is nearly of so-called "Type-IB" point-on-line coincidence[32] with a 6% lattice mismatch, as illustrated in Figure 1c. Moreover, the crystallographic coherence length of the C_{60} overlayers grown at room temperature (RT) was found to exceed 100 nm in the in-plane directions.[33] The well-defined interface between Pn-SC and C_{60} is ideally suited to study kinetic effects[34] in the growth of the topical donor–acceptor heterojunction. We herein demonstrate the crystallographic coherence of the C_{60} overlayers on the Pn-SC as a function of the growth temperature through systematic

Prof. Y. Nakayama, R. Tsuruta
Department of Pure and Applied Chemistry
Tokyo University of Science
2641 Yamazaki, Noda 278-8510, Japan
E-mail: nkym@rs.tus.ac.jp

Dr. A. Hinderhofer, Prof. K. Broch, Dr. A. Gerlach, Prof. F. Schreiber
Institut für Angewandte Physik
Eberhard Karls Universität Tübingen
Auf der Morgenstelle 10, 72076 Tübingen, Germany

The ORCID identification number(s) for the author(s) of this article can be found under https://doi.org/10.1002/admi.201800084.

DOI: 10.1002/admi.201800084

Y. Mizuno
Graduate School of Advanced Integration Science
Chiba University
1-33 Yayoi-cho, Inage-ku, Chiba 263-8522, Japan

Dr. T. Koganezawa
Industrial Application Division
Japan Synchrotron Radiation Research Institute (JASRI)
1-1-1 Kouto, Sayo, Hyogo 679-5198, Japan

Dr. T. Hosokai
National Metrology Institute of Japan
National Institute of Advanced Industrial Science and Technology
Tsukuba Central 2, 1-1-1 Umezono, Tsukuba, Ibaraki 305-8568, Japan

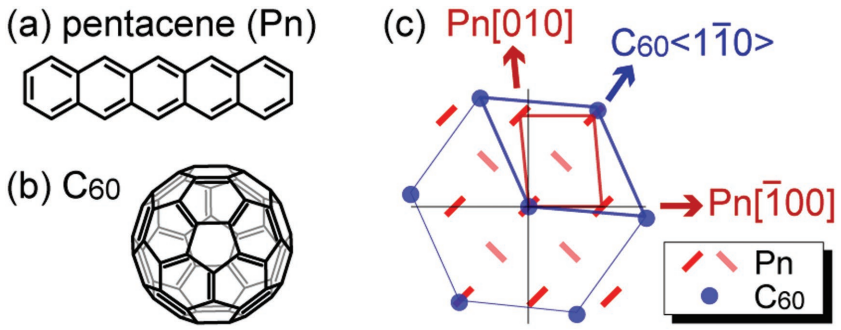

Figure 1. a) Molecular structure of pentacene. b) Molecular structure of C_{60}. c) The epitaxial interlattice relationship of the C_{60}/pentacene interface as reported in Ref. [31]. The in-plane molecular arrangement of the Pn-SC surface is represented with bars where two inequivalent Pn molecules in a unit cell are distinguished by the direction and color tone of the symbols, while that of fcc-(111) surface of C_{60} is shown with circles.

grazing-incidence X-ray diffraction (GIXD) and X-ray reflectivity (XRR) investigations. Proportional increase of the in-plane mean crystallite size of C_{60} with the growth temperature suggests importance of surface diffusion processes of the C_{60} molecules on the Pn-SC surface as a leading factor for determination of the heterojunction structures.

2. Results and Discussion

Figure 2 insets show typical AFM images of the Pn-SC samples covered with 20 nm-thick C_{60} overlayers grown at various substrate temperatures, i.e., 160, 300, and 370 K. C_{60} forms grains on the Pn-SC surface in the case of RT (300 K) growth as reported previously,[23,31] and it was found that the lateral sizes and shapes of these grains vary depending on the growth temperature. Histograms of the grain sizes derived from the respective AFM images indicate the evolution of the average size (average diameter of the equiareal circle $\bar{d}$) and standard deviation (σ) of the C_{60} grains depending on the growth temperature, as shown in Figure 2. In comparison to the case of RT growth ($\bar{d}$ = 157 nm, σ = 52 nm), growth of the C_{60} overlayers at low temperature (160 K) resulted in a drastic decrease in the grain size ($\bar{d}$ = 72 nm) and a more uniform size distribution of the grains (σ = 29 nm), while raising the growth temperature (370 K) increases the grain size ($\bar{d}$ = 181 nm) and broadens the size distribution (σ = 64 nm). In addition, growth of the C_{60} overlayers at increased temperatures transforms the typical shapes of the grains into table-like islands with very flat tops and straight peripheries. The large $\bar{d}$ and polygonal shapes of the grains can be regarded as signs of improved crystallinity of the C_{60} overlayers on the Pn-SC by raising the growth temperature.

In comparison to the RT-grown C_{60}/Pn-SC sample, typical heights of the grains are notably enhanced to greater than 10 nm for the high temperature (HT) growth, as shown in Figure S1 (Supporting Information). This implies that the HT-grown C_{60}/Pn-SC heterostructure is consisting of the crystalline C_{60} "islands" on bare Pn-SC "sea." In contrast, as seen in Figure 2a, the C_{60} grains formed at low growth temperatures look like small particles and regular shapes are hardly recognized. This suggests that the crystallization of the C_{60} overlayers is significantly impeded by reduction of the growth temperature.

As reported previously, C_{60} nucleates in an fcc lattice with the [111] direction perpendicular to the surface and the $<1\bar{1}0>$ direction parallel to the [$\bar{1}$10] axis of the "single crystal phase" pentacene.[31] In that arrangement, the C_{60} surface exhibits hexagonal symmetry; and thus, in-plane diffraction spots from C_{60} appear with a 60° periodicity when rotating the sample around ϕ. The aforementioned epitaxial interlattice relationship gives $\{2\bar{2}0\}$ diffraction spots of C_{60} on the Pn-SC $(00\bar{1})$ surface at six ϕ angles in the 60° intervals (ϕ = 39.8, 99.8, 159.8, 219.8, 279.8, and 339.8°) under the present measurement conditions. **Figure 3**a shows the ϕ-dependence of the $C_{60}\{2\bar{2}0\}$ scattering intensity derived from the present 2D GIXD (2D-GIXD) results, where the intensities are normalized by the 360°-averaged intensity of the respective samples and are plotted on a logarithmic scale as the radial axis. In these plots, the origin of ϕ is taken at the angle where the Pn-SC(100) diffraction spot appears, and the six ϕ angles at which the diffraction spot

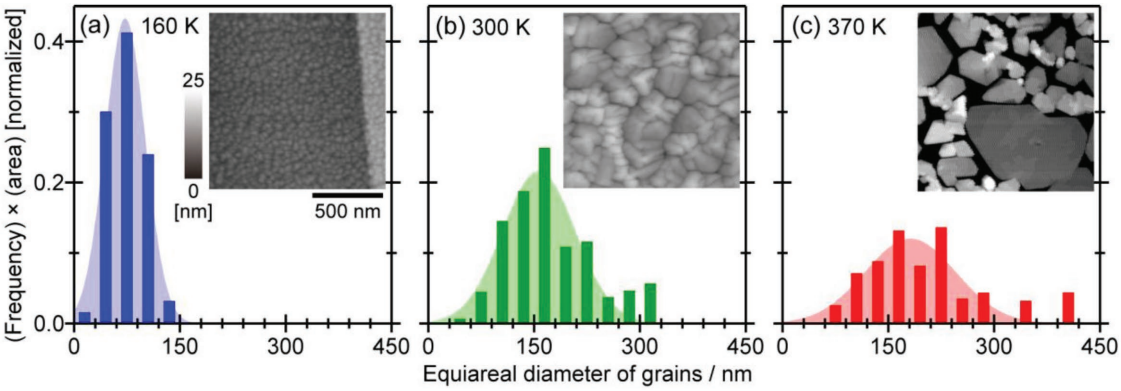

Figure 2. Histograms of the grain size of the 20 nm-thick epitaxial overlayers of C_{60} on the Pn-SC prepared at a) 160 K, b) 300 K, and c) 370 K, derived from AFM images. Least-squares fitting results assuming the normal distribution are represented as light-colored curves. (Insets) AFM images of the respective samples. The horizontal and vertical scales of these three images are equal.

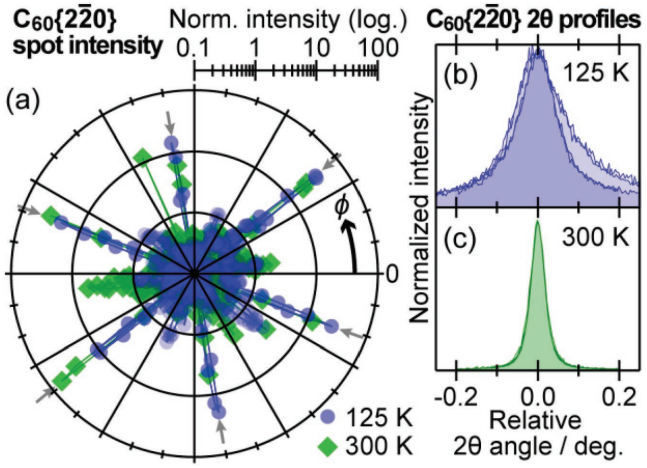

Figure 3. a) A polar plot representing the spot intensity at the q position corresponding to the fcc-$C_{60}\{2\bar{2}0\}$ diffraction depending on the sample azimuthal angle ϕ of the 20 nm-thick C_{60}/Pn-SC samples grown at 125 K (circles) and 300 K (diamonds). b) 2θ-scan profiles of four $C_{60}\{2\bar{2}0\}$ diffraction spots of the C_{60}/Pn-SC sample grown at 125 K. c) 2θ-scan profiles of four $C_{60}\{2\bar{2}0\}$ diffraction spots of the RT-grown C_{60}/Pn-SC.

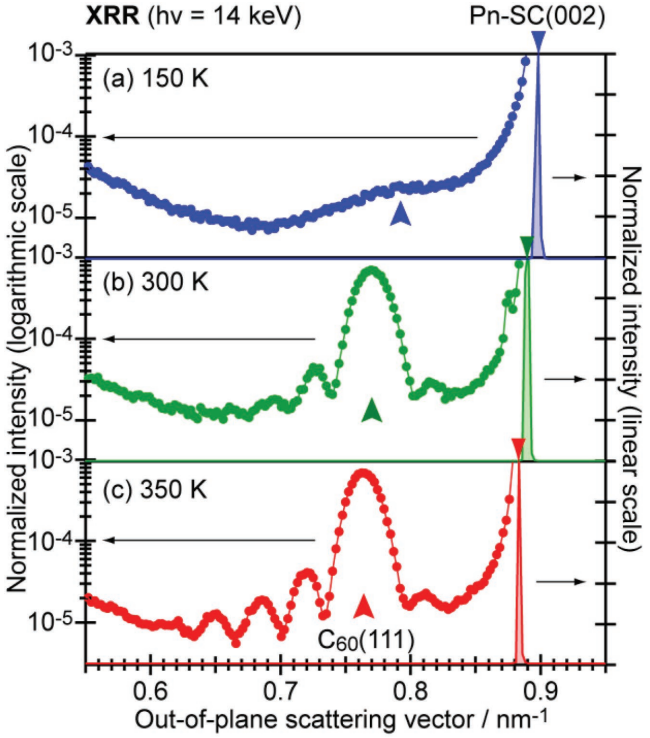

Figure 4. XRR curves of 20 nm-thick C_{60} overlayers on the Pn-SC formed at a) 150 K, b) 300 K, and c) 350 K. The intensities are normalized at the Pn-SC(002) Bragg reflection peaks (downward wedge marks) of the respective samples, and the q_z ranges around the C_{60}(111) reflections are magnified on a logarithmic scale. The C_{60}(111) positions are indicated by upward arrows.

appeared are indicated by gray arrows. The present results confirm that the identical epitaxial relationship between C_{60} overlayers and Pn-SC is retained even for the C_{60}/Pn-SC grown at 125 K. This indicates that even though reduced crystallinity of C_{60} is suggested from AFM observations, the LT-grown C_{60} overlayers are not amorphous nor randomly oriented crystallites. Instead, C_{60} still forms epitaxial overlayers of a unique crystallographic orientation on the Pn-SC surface even under low growth temperature conditions.

Figure 3b,c shows the in-plane 2θ-profiles of four $C_{60}\{2\bar{2}0\}$ diffraction spots (out of six excluding two coinciding another diffraction signal from the Pn-SC[33]) of the C_{60}/Pn-SC samples grown at 125 and 300 K, respectively. The full-width of the half-maximum (FWHM) of the diffraction spots was 0.039° on average for the present RT-grown sample, a value that is consistent with our previous report.[33] On the other hand, the spot profiles of the LT-grown C_{60}/Pn-SC exhibited significant broadening in comparison to the case of the RT-growth. The average FWHM of the four $C_{60}\{2\bar{2}0\}$ diffraction spots was 0.13° for this LT-grown sample. By the Scherrer equation, this means that the in-plane mean crystallite size of the C_{60} overlayers grown at 125 K shrinks by about a factor of three compared to that of the RT-grown overlayers. This trend is confirmed for other growth temperatures as shown in Figure S2 (Supporting Information). A decrease in the growth temperature also disturbs the uniformity of in-plane crystalline alignments of the C_{60} overlayers, as suggested by broadening of the ϕ-dependence of the $C_{60}\{2\bar{2}0\}$ diffraction intensities (Figure S3, Supporting Information).

We emphasize that the above GIXD and nc-AFM experiments were done at RT even for the LT-grown C_{60}/Pn-SC samples; namely, these C_{60} overlayers formed at LT had experienced postannealing to RT prior to the measurements. Striking differences in the present AFM and GIXD results depending on the growth temperature even after the postannealing mean that the crystalline domain size of C_{60}/Pn-SC is mostly determined by events during growth driven by kinetic factors, e.g., nucleation density of the C_{60} molecules in succession to diffusion on the Pn-SC surface, rather than the thermal equilibrium.

Crystallinity along the surface normal is deduced from the profiles of the out-of-plane diffraction spots. **Figure 4** shows the XRR data representing the C_{60}(111) and Pn-SC(002) spots of 20 nm-thick C_{60} overlayers grown at various temperatures. The spot positions of the Pn-SC(002) Bragg reflection (downward wedge marks) are shifted to lower q, since an increase in temperature results in thermal expansion of the sample. At RT (Figure 4b), the C_{60}(111) reflection (upward arrow) at the out-of-plane scattering vector (q_z) of 0.770 nm^{-1} is accompanied by Laue fringes on both sides indicating good crystallinity and crystal orientation of the overlayers, as reported previously.[31] The fringe structures as well as the main peak profile are more pronounced for the C_{60} overlayers formed at 350 K, as shown in Figure 4c, suggesting further improvement of the crystallinity. For the C_{60}/Pn-SC sample grown at 150 K, the C_{60}(111) Bragg reflection is resolvable but very broad (Figure 4a). This observation means that C_{60} preserves the (111) orientation even when the growth temperature is low but its crystallographic coherence is disturbed in the direction perpendicular to the substrate. It is worth mentioning that postannealing of the LT-grown C_{60} overlayers to RT did not significantly improve the crystal quality (Figure S4, Supporting Information). This also demonstrates the importance of kinetic factors in comparison

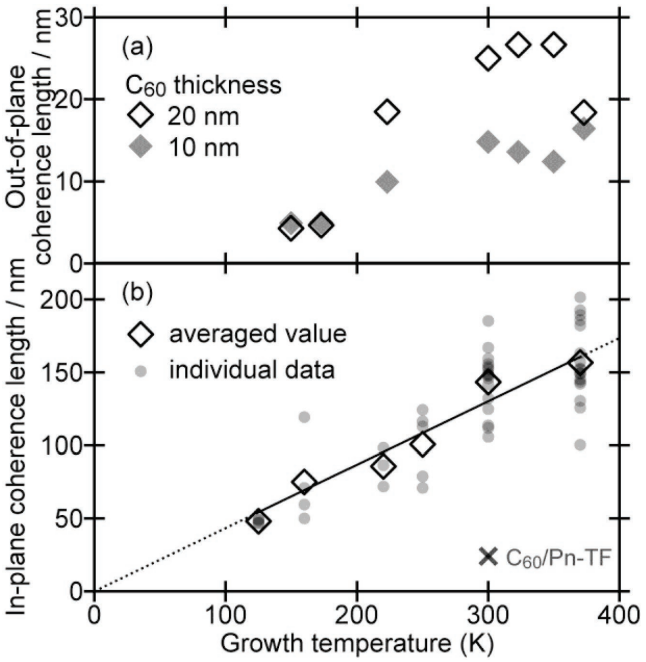

Figure 5. a) Out-of-plane coherence length of the C_{60} overlayers derived from the XRR spot width of the C_{60}(111) peaks on the 10 nm-thick (filled diamonds) and 20 nm-thick (open symbols) C_{60}/Pn-SC plotted as a function of the growth temperature. b) In-plane coherence length derived from the HR-GIXD width of the $C_{60}\{2\bar{2}0\}$ spots on the 20 nm-thick C_{60}/Pn-SC depending on the growth temperature. The in-plane coherence length of the C_{60} overlayers formed on pentacene thin films is also represented by a cross mark.

to thermal equilibrium conditions for the crystallinity of the studied molecular heterojunction.

Figure 5 shows the evolution of the mean crystallite sizes, i.e., the crystallographic coherence length, along the out-of-plane (q_z) and in-plane (q_{xy}) directions of C_{60} on Pn-SC being evaluated from spot widths of the C_{60}(111) and $\{2\bar{2}0\}$ reflections, respectively. In Figure 5b, the gray circles represent estimated values from individual diffraction spots and the open diamonds correspond to the averaged values of these data points from several samples grown at each growth temperature. A thin line represents a linear fit of the averaged values as a function of the growth temperature. Based on these trends together with the AFM observations, growth manners of the epitaxial C_{60} overlayers are summarized as shown in **Figure 6** according to the following discussion.

In the out-of-plane direction, roughly three types of growth behaviors are recognized from the temperature dependence (Figure 5a). For growth temperatures below 200 K, the coherence length is restricted to ≈5 nm regardless of the total C_{60} layer thickness. This strongly suggests that the C_{60} overlayers formed at these temperatures are not single crystalline but are agglomerations of small crystalline domains with stacking faults (Figure 6a, inset). It has to be emphasized that, even though crystalline coherence in the out-of-plane direction is disturbed for these LT-grown C_{60} overlayers, the in-plane epitaxial relationship is maintained across the boundaries of these out-of-plane domain stacks, as indicated by the 2D-GIXD results, presumably because the in-plane nearest-neighbor direction of the C_{60} molecules aligns to the molecular arrangement just beneath. In the temperature range of 200–350 K, the coherence length of the 20 nm-thick C_{60} overlayers is roughly doubled compared to those of the 10 nm-thick samples, and the derived values agree with the nominal thicknesses well. This strongly suggests that crystalline coherence is realized throughout the entire thickness of the C_{60} overlayers grown in this temperature range (Figure 6b). A coherence length exceeding the nominal C_{60} thickness at elevated growth temperature may be caused by the "sea-island" structure observed in the AFM images (Figure 2c, inset; Figure S1c, Supporting Information) as drawn in Figure 6c. For further increased growth temperature (>350 K), the sudden drop of the mean crystallite size for the 20 nm-thick C_{60}/Pn-SC may be ascribed to competing desorption of C_{60} and/or damages to the sample due to long term heating (see Figure S3d in the Supporting Information).

On the other hand, the mean crystallite size (coherence length) in the in-plane directions exhibited a monotonous increase for an increase of growth temperature as shown in Figure 5b. The in-plane coherence length of the epitaxial C_{60} overlayers derived from the high-resolution GIXD (HR-GIXD) results exceeded 150 nm on average for the heated (370 K) Pn-SC, while it was smaller than 50 nm for the low temperature growth (125 K). It is noteworthy that the in-plane coherence length of RT-grown C_{60} overlayers on Pn thin films (Pn-TFs) was estimated to be 23 nm (a cross mark in Figure 5b),[33] which is still smaller than the LT-grown case on the Pn-SC. As clearly seen in Figure 5b, the estimated in-plane coherence length is approximately proportional to the growth temperature. This suggests that the in-plane crystalline domain size of the C_{60}/Pn-SC heterojunction is dominated by the diffusion constant, which is proportional to the temperature under an assumption of the Einstein-Smoluchowski relation, of the C_{60} molecules on the Pn-SC surface. From the opposite viewpoint, the maximum crystalline grain size of the C_{60}/Pn-SC heterojunction is expected by the enhancement of the diffusion length of the C_{60} molecules on the Pn-SC. A reduced diffusion length at low temperatures leads to a large nucleation density of the C_{60} molecules and a shorter mean distance between the nuclei, which restricts the growth of crystalline domain size even though all individual crystallites align epitaxially to the Pn-SC surface lattice.

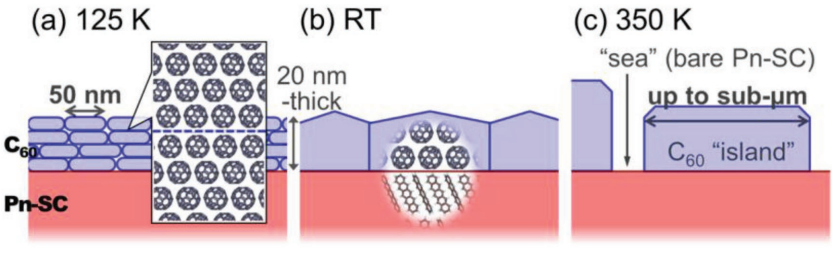

Figure 6. Schematic drawings of the growth of C_{60} on Pn-SC depending on the growth temperature.

While elevating the growth temperature is effective to extend the grain size, further improvement of the crystallinity by this route is unlikely due to the limited thermal stability of the C_{60} overlayers as well as that of the Pn-SC substrate, as suggested by the present study. Another strategy may be the suppression of factors hindering the surface diffusion. Since step edges of the substrate behave as diffusion barriers for adsorbates, a reduction of the step density through optimized preparation procedures for the Pn-SC substrates may lead to an increase of the crystalline grain size of the C_{60} overlayers. In addition, impurities are presumably obstacles against the surface diffusion. Sequential sublimation of the C_{60} source material and growth of the epitaxial overlayres using a vacuum chamber built in a glove box (inert atmosphere) may lead to a maximization of the crystal quality of the C_{60} overlayers through elimination of admixing impurities.[35,36] It is also noteworthy that the present Pn-SC substrates experienced exposure to the ambient air and light, and it is known that a few percent of oxides are generated at the Pn-SC surface by ambient exposure.[37] Formation of the C_{60} overlayers on the Pn-SC clean surface prepared by, e.g., cleavage in a vacuum[38] may open a new route for realizing highly-crystallized epitaxial C_{60}/Pn-SC heterojunctions.

3. Conclusion

In the present work, evolution of the epitaxial C_{60} overlayers formed on the Pn-SC surface, depending on the growth temperature (125–370 K), is investigated by means of nc-AFM and surface X-ray diffraction techniques. It is confirmed that C_{60} aligns its fcc-$[1\bar{1}0]$ direction along the $[\bar{1}10]$ axis of the Pn-SC independent of the growth temperature. On the other hand, the crystallinity of the C_{60} overlayers strongly depends on the growth temperature. When C_{60} is grown at low temperatures below 200 K, the out-of-plane mean crystallite size of the C_{60} overlayers is limited to around 5 nm even though the total thickness is above 10 nm. This suggests that the overlayers are not coherently ordered in the out-of-plane direction even though the in-plane lattice orientation is uniquely preserved throughout the C_{60} overlayers. Also in the in-plane directions, the coherence length is diminished to ≈50 nm for a growth temperature of 125 K. Elevating the growth temperature results in coherent crystalline overlayers of C_{60} in the out-of-plane direction and an increase of the in-plane mean crystallite size to over 150 nm at a growth temperature of 370 K. The present result also suggests that the crystallinity of the C_{60}/Pn-SC molecular heterojunction is mostly dominated by surface diffusion of the adsorbed C_{60} molecules during growth rather than postgrowth thermal treatments.

4. Experimental Section

AFM and GIXD Measurements: The Pn-SC substrates bonded onto Si wafers were prepared by the same procedures reported previously.[31,33] For the AFM and GIXD experiments, 20 nm-thick films of C_{60} were deposited onto the Pn-SC substrates which are kept at various temperatures (125–370 K) under ultrahigh vacuum (UHV) conditions. The C_{60} source (99.98%) was purchased from ATR Company and used without further purification. The material was introduced in a quartz crucible which was set at ≈0.2 m far from the Pn-SC sample, where an evaporation rate was set at 0.03 nm s^{-1}. The prepared C_{60}/Pn-SC samples were taken to ambient atmosphere for the successive measurements. AFM images were collected by using an nc-AFM apparatus (SPA-400, SII). GIXD measurements were conducted at BL46XU of SPring-8. The X-ray wave length and glancing angle were set to be 0.10 nm and 0.12°, respectively. The in-plane crystallographic relationship between the C_{60} overlayers and the Pn-SC surface lattice was derived from changes of the 2D-GIXD patterns depending on the sample azimuthal angle ϕ, where the sample orientation at which the Pn-SC (100) diffraction spot was observed is defined as the origin of ϕ ($\phi = 0°$) hereafter. The experimental setup of the 2D-GIXD measurements was previously reported.[31] Note that the surface index of the plate-shaped Pn-SC is either (001) or $(00\bar{1})$, and these two faces can be distinguished through the ϕ-dependence of the 2D-GIXD patterns of the Pn-SC[31]; all the GIXD data shown in the present paper were from the C_{60} overlayers formed on the Pn-SC $(00\bar{1})$ side. The mean crystallite size, namely the crystallographic coherence length, along the in-plane directions can be estimated from the width of the diffraction spot profiles in the 2θ direction. In the present work, the 2θ-profiles were obtained through HR-GIXD measurements by using a NaI scintillation counter and a Ge(111) analyzer crystal for the sake of evaluating the in-plane mean crystallite sizes of the C_{60} overlayers.[33] The AFM and GIXD measurements were carried out at RT.

XRR Measurements: XRR was performed "in situ" in a step-by-step manner during the growth of the C_{60} overlayers intermittently in a home-built portable UHV chamber equipped with a Be window and mounted on a goniometer.[39,40] For these experiments, C_{60} was evaporated from a Knudsen cell set at 655 (± 5) K (a deposition rate of 0.002 nm s^{-1}) on the temperature-controlled Pn-SC surfaces. The measurements were done at an X-ray energy of 14 keV at the MS Surface Diffraction beamline[41] of the Swiss Light Source. It is worth mentioning that exposure of the C_{60}/Pn-SC samples to the ambient air and light does not induce any notable change in their morphological and crystallographic structures, as confirmed previously.[31] In addition, increasing the deposition rate of C_{60} from 0.002 to 0.017 nm s^{-1} brought about merely a weak change in the XRR signal (Figure S5, Supporting Information). The present XRR measurements were conducted at the respective growth temperature unless otherwise noted.

Supporting Information

Supporting Information is available from the Wiley Online Library or from the author.

Acknowledgements

The authors would like to thank Prof. Hisao Ishii (Chiba University) and Dr. Hiroshi Itoh (AIST) for supporting the AFM experiments and analyses, and Heiko Frank (Universität Tübingen) and Valentina Belova (Universität Tübingen) for their help during the XRR experiments. A part of this work was done under the approval of JASRI (Proposal 2015A1685 and 2015B1624 as collaborating proposals with Keysight Technologies) and of the Paul Scherrer Institute (Proposals 20141165 and 20150468). Financial supports from KAKENHI Grant Numbers JP15H05498, JP16K14102, and JP16K17975 of the Japan Society for the Promotion of Science (JSPS) and the Start-up Fund for Young Faculties of Tokyo University of Science are gratefully acknowledged. This work is also partially supported by The Precise Measurement Technology Promotion Foundation, Iketani Science and Technology Foundation, and the DFG.

Conflict of Interest

The authors declare no conflict of interest.

Keywords

donor–acceptor interface, heteroepitaxy, organic semiconductor, p–n junction, surface diffusion

Received: January 17, 2018
Revised: February 19, 2018
Published online: April 19, 2018

[1] S. Machida, Y. Nakayama, S. Duhm, Q. Xin, A. Funakoshi, N. Ogawa, S. Kera, N. Ueno, H. Ishii, *Phys. Rev. Lett.* **2010**, *104*, 156401.
[2] Y. Nakayama, Y. Uragami, S. Machida, K. R. Koswattage, D. Yoshimura, H. Setoyama, T. Okajima, K. Mase, H. Ishii, *Appl. Phys. Express* **2012**, *5*, 111601.
[3] Y. Nakayama, Y. Mizuno, M. Hikasa, M. Yamamoto, M. Matsunami, S. Ideta, K. Tanaka, H. Ishii, N. Ueno, *J. Phys. Chem. Lett.* **2017**, *8*, 1259.
[4] R. W. I. de Boer, M. E. Gershenson, A. F. Morpurgo, V. Podzorov, *Phys. Status Solidi* **2004**, *201*, 1302.
[5] M. E. Gershenson, V. Podzorov, *Rev. Mod. Phys.* **2006**, *78*, 973.
[6] T. Hasegawa, J. Takeya, *Sci. Technol. Adv. Mater.* **2009**, *10*, 24314.
[7] A. Dodabalapur, H. E. Katz, L. Torsi, R. C. Haddon, *Science* **1995**, *269*, 1560.
[8] H. Alves, A. S. Molinari, H. Xie, A. F. Morpurgo, *Nat. Mater.* **2008**, *7*, 574.
[9] S. S. Cheng, P. Y. Huang, M. Ramesh, H. C. Chang, L. M. Chen, C. M. Yeh, C. L. Fung, M. C. Wu, C. C. Liu, C. Kim, H. C. Lin, M. C. Chen, C. W. Chu, *Adv. Funct. Mater.* **2014**, *24*, 2057.
[10] R. R. Lunt, J. B. Benziger, S. R. Forrest, *Adv. Mater.* **2010**, *22*, 1233.
[11] H. Najafov, B. Lee, Q. Zhou, L. C. Feldman, V. Podzorov, *Nat. Mater.* **2010**, *9*, 938.
[12] A. C. Jakowetz, M. L. Böhm, J. Zhang, A. Sadhanala, S. Huettner, A. A. Bakulin, A. Rao, R. H. Friend, *J. Am. Chem. Soc.* **2016**, *138*, 11672.
[13] V. Abramavicius, V. Pranculis, A. Melianas, O. Inganäs, V. Gulbinas, D. Abramavicius, *Sci. Rep.* **2016**, *6*, 32914.
[14] D. A. Vithanage, A. B. Matheson, V. Pranculis, G. J. Hedley, S. J. Pearson, V. Gulbinas, I. D. W. Samuel, A. Ruseckas, *J. Phys. Chem. C* **2017**, *121*, 14060.
[15] A. Hinderhofer, F. Schreiber, *ChemPhysChem* **2012**, *13*, 628.
[16] J. Wagner, M. Gruber, A. Hinderhofer, A. Wilke, B. Bröker, J. Frisch, P. Amsalem, A. Vollmer, A. Opitz, N. Koch, F. Schreiber, W. Brütting, *Adv. Funct. Mater.* **2010**, *20*, 4295.
[17] B. A. Collins, J. R. Tumbleston, H. Ade, *J. Phys. Chem. Lett.* **2011**, *2*, 3135.
[18] S. Yoo, B. Domercq, B. Kippelen, *Appl. Phys. Lett.* **2004**, *85*, 5427.
[19] K. Itaka, M. Yamashiro, J. Yamaguchi, M. Haemori, S. Yaginuma, Y. Matsumoto, M. Kondo, H. Koinuma, *Adv. Mater.* **2006**, *18*, 1713.
[20] I. Salzmann, S. Duhm, R. Opitz, R. L. Johnson, J. P. Rabe, N. Koch, *J. Appl. Phys.* **2008**, *104*, 114518.
[21] B. R. Conrad, J. Tosado, G. Dutton, D. B. Dougherty, W. Jin, T. Bonnen, A. Schuldenfrei, W. G. Cullen, E. D. Williams, J. E. Reutt-Robey, S. W. Robey, *Appl. Phys. Lett.* **2009**, *95*, 213302.
[22] T. Breuer, G. Witte, *ACS Appl. Mater. Interfaces* **2013**, *5*, 9740.
[23] M. Yamamoto, Y. Nakayama, Y. Uragami, H. Kinjo, Y. Mizuno, K. Mase, K. R. Koswattage, H. Ishii, *e-J. Surf. Sci. Nanotechnol.* **2015**, *13*, 59.
[24] T. Breuer, A. Karthäuser, G. Witte, *Adv. Mater. Interfaces* **2016**, *3*, 1500452.
[25] R. Cantrell, P. Clancy, *Surf. Sci.* **2008**, *602*, 3499.
[26] S. Verlaak, D. Beljonne, D. Cheyns, C. Rolin, M. Linares, F. Castet, J. Cornil, P. Heremans, *Adv. Funct. Mater.* **2009**, *19*, 3809.
[27] M. Linares, D. Beljonne, J. Cornil, K. Lancaster, J.-L. Brédas, S. Verlaak, A. Mityashin, P. Heremans, A. Fuchs, C. Lennartz, J. Idé, R. Méreau, P. Aurel, L. Ducasse, F. Castet, *J. Phys. Chem. C* **2010**, *114*, 3215.
[28] Y.-T. Fu, C. Risko, J.-L. Brédas, *Adv. Mater.* **2013**, *25*, 878.
[29] Y. M. Acevedo, R. A. Cantrell, P. G. Berard, D. L. Koch, P. Clancy, *Langmuir* **2016**, *32*, 3045.
[30] S. M. Ryno, Y.-T. Fu, C. Risko, J.-L. Brédas, *ACS Appl. Mater. Interfaces* **2016**, *8*, 15524.
[31] Y. Nakayama, Y. Mizuno, T. Hosokai, T. Koganezawa, R. Tsuruta, A. Hinderhofer, A. Gerlach, K. Broch, V. Belova, H. Frank, M. Yamamoto, J. Niederhausen, H. Glowatzki, J. P. Rabe, N. Koch, H. Ishii, F. Schreiber, N. Ueno, *ACS Appl. Mater. Interfaces* **2016**, *8*, 13499.
[32] D. E. Hooks, T. Fritz, M. D. Ward, *Adv. Mater.* **2001**, *13*, 227.
[33] R. Tsuruta, Y. Mizuno, T. Hosokai, T. Koganezawa, H. Ishii, Y. Nakayama, *J. Cryst. Growth* **2017**, *468*, 770.
[34] T. Michely, J. Krug, *Islands, Mounds and Atoms*, Springer, Berlin Heidelberg **2004**.
[35] K. Sakai, M. Hiramoto, *Mol. Cryst. Liq. Cryst.* **2008**, *491*, 284.
[36] C. Ohashi, S. Izawa, Y. Shinmura, M. Kikuchi, S. Watase, M. Izaki, H. Naito, M. Hiramoto, *Adv. Mater.* **2017**, *29*, 1605619.
[37] Y. Nakayama, Y. Uragami, M. Yamamoto, K. Yonezawa, K. Mase, S. Kera, H. Ishii, N. Ueno, *J. Phys. Condens. Matter* **2016**, *28*, 94001.
[38] Y. Mizuno, M. Yamamoto, H. Kinjo, K. Mase, H. Ishii, K. K. Okudaira, H. Yoshida, Y. Nakayama, *Mol. Cryst. Liq. Cryst.* **2017**, *648*, 216.
[39] K. A. Ritley, B. Krause, F. Schreiber, H. Dosch, *Rev. Sci. Instrum.* **2001**, *72*, 1453.
[40] T. Hosokai, A. Gerlach, A. Hinderhofer, C. Frank, G. Ligorio, U. Heinemeyer, A. Vorobiev, F. Schreiber, *Appl. Phys. Lett.* **2010**, *97*, 63301.
[41] P. R. Willmott, D. Meister, S. J. Leake, M. Lange, A. Bergamaschi, M. Böge, M. Calvi, C. Cancellieri, N. Casati, A. Cervellino, Q. Chen, C. David, U. Flechsig, F. Gozzo, B. Henrich, S. Jäggi-Spielmann, B. Jakob, I. Kalichava, P. Karvinen, J. Krempasky, A. Lüdeke, R. Lüscher, S. Maag, C. Quitmann, M. L. Reinle-Schmitt, T. Schmidt, B. Schmitt, A. Streun, I. Vartiainen, M. Vitins, X. Wang, R. Wullschleger, *J. Synchrotron Radiat.* **2013**, *20*, 667.

